

---

# Spectral2Spectral: Image-spectral Similarity Assisted Spectral CT Deep Reconstruction without Reference

Yonghui Li<sup>1</sup>, Peng He<sup>1</sup>, Peng Feng<sup>1</sup>, Xiaodong Guo<sup>1</sup>, Weiwen Wu<sup>2</sup> and Hengyong Yu<sup>3</sup>

<sup>1</sup> Key Lab of Optoelectronic Technology and Systems of the Education Ministry of China, Chongqing University, Chongqing, China  
(e-mail: 20165953@cqu.edu.cn, penghe@cqu.edu.cn)

<sup>2</sup>The School of Biomedical Engineering, Sun Yat-Sen University, Shenzhen, Guangdong, China (e-mail: wuweiw7@mail.ssu.edu.cn)

<sup>3</sup>Department of Electrical and Computer Engineering, University of Massachusetts Lowell, MA, USA (email: hengong-yu@ieee.org)

**Abstract-** The photon-counting detector (PCD) based spectral computed tomography attracts much more attentions since it has the capability to provide more accurate identification and quantitative analysis for biomedical materials. The limited number of photons within narrow energy-bin leads to low signal-noise ratio data. The existing supervised deep reconstruction networks for CT reconstruction are difficult to address these challenges. In this paper, we propose an iterative deep reconstruction network to synergize model and data priors into a unified framework, named as Spectral2Spectral. Our Spectral2Spectral employs an unsupervised deep training strategy to obtain high-quality images from noisy data with an end-to-end fashion. The structural similarity prior within image-spectral domain is refined as a regularization term to further constrain the network training. The weights of neural network are automatically updated to capture image features and structures with iterative process. Three large-scale preclinical datasets experiments demonstrate that the Spectral2spectral reconstruct better image quality than other state-of-the-art methods.

**Keywords:** Spectral CT, image reconstruction, unsupervised learning, neural network, iterative reconstruction

## I. Introduction

The photon-counting detector (PCD) based spectral CT system has strong ability to identify an absorption property within available energy ranges, demonstrating a great potential in contrast resolution enhancement, material identification, and quantitative analysis of biomedical soft tissues. PCD uses selectable energy thresholds to record energies of different x-ray photons with appropriate image post-processing techniques. Specifically, there are lots of quantum noises in acquired projections within an narrow energy bin, resulting in lower signal-noise ratio (SNR) in the reconstructed images. Therefore, how to reconstruct high-quality CT images from noisy projections is a challenge in the field of spectral CT.

In recent years, compressed sensing [1, 2] based iterative reconstruction algorithms have

---

been developed, which can reconstruct high-quality spectral CT images from noisy or incomplete projection data. For example, Zhang *et al.* applied a tensor dictionary learning (TDL) [3] technique to improve image quality of spectral CT reconstruction based on the similarity of images among different energy bins. Wu *et al.* introduced an image gradient  $l_0$ -norm into TDL to reconstruct low-dose spectral CT images, which is very effective to deal with image artifacts and noises [4]. In addition, other compressed sensing based reconstruction methods were also developed for spectral CT, including [5], [6] and [7], *etc.* Besides, there are other type spectral CT reconstruction algorithms, such as maximum a posteriori expectation-maximization (MAP-EM-DD) [8] and non-convex primal-dual (NCPD) algorithms [9].

Currently, deep learning (DL) technology has been widely used in the fields of biomedical imaging and tomographic reconstruction [10]. In the post-processing tomographic reconstruction, Chen *et al.* [11, 12] proposed a low-dose CT reconstruction method based on deep learning. FBPCnvNet [13] used U-Net to improve image quality over raw FBP reconstructed images [14]. In addition, DD-Net [15], wavelet-transform-base U-net [16, 17], BCD-Net [18], and others [19] were further developed. Although these methods can obtain better results with good efficiency, they require the ground truths as the training labels. Regarding the end-to-end tomographic reconstruction, He *et al.* [20] designed a novel framework to approximate the Radon inversion. Zhu *et al.* [21] proposed a fully manifold encoding-decoding convolutional architecture. However, these reconstruction methods require large amounts of paired data and high computing costs, particularly the large GPU memory. Since it is very difficult to obtain high-quality image for spectral CT, these deep reconstruction networks fail to achieve good reconstructed image quality. Hence, there are some deep reconstruction methods were developed to reconstruct spectral CT images without reference. For example, Niu *et al.* presented a Noise2Sim unsupervised post-processing network [22]. Noise2Sim uses the similarity from the neighboring slices as a prior knowledge to help network training. The main contribution is that Noise2Sim presents a new solution to construct pseudo-label for spectral CT denoising. However, it is difficult to find two similar images for spectral CT images, especially in fan-beam geometry. Besides, the reconstruction performance is also limited by the spatial similarity from two slices. Finally, it is one of post-processing deep denoising networks, and its performance is limited by data consistency.

Inspired by the Noise2Sim, we propose a Spectral2Spectral unsupervised reconstruction network, which synergizes the model knowledge (i.e., simultaneous iterative reconstruction technique (SIRT) [23]) and data prior into a unified mathematical model. It reconstructs high-quality images from measurement data, and an unsupervised neural network is developed to optimize the reconstructed images. First, Spectral2Spectral incorporates a deep learning network into an iterative reconstruction framework to achieve a stable and reliable deep reconstruction solution. Second, the quality of reconstructed image is improved with an advanced unsupervised network by designing a novel loss function with the unique properties of spectral CT. Third, the proposed reconstruction model updates the weights automatically in the iterative process to adaptively optimize the reconstructed images.

The main unique contributions of this study are threefold. First, we reshape the spectral CT mathematical reconstruction model and derive a general optimized solution. A deep neural network is further introduced to approximate intermediate iterative image and

---

enhance the effectiveness of the iterative reconstruction. The network weight parameters are automatically updated with iteration number, which benefits to adaptive learn image structures and features. Second, we innovatively develop an unsupervised iterative learning for spectral CT reconstruction. Traditional deep learning-based CT reconstruction methods require clean labeled datasets. The developed unsupervised iterative learning releases the requirement of high-quality reference by constructing pseudo-labels. Here, the pseudo-labels are constructed from the spectral CT images themselves. The noises in spectral CT are reduced with the help of pseudo-labels. Third, based on image-spectral similarity within spectral CT, a priori knowledge is incorporated into our iterative reconstruction framework to improve the image quality. Because spectral CT images have high structural similarity across the energy domain, a loss function is developed to compute the image-spectral similarity to improve image details and sharp image edges.

The rest of the paper is organized as follows. In section II, we first briefly introduce CT reconstruction theory and representative unsupervised networks. Then, we describe our proposed Spectral2spectral deep reconstruction network in details. In section III, the specific experimental design, results and ablation studies are presented and analyzed. In the last section, we discuss some relevant issues and conclude the paper.

## II. Method

### A. Theoretical Background

#### (1) Unsupervised Denoising

Recently, convolutional neural networks (CNNs) provide powerful tools for image denoising. Noise2Noise [24] was first developed by Lehtinen *et al.* to train a deep denoiser using several noisy observations of the same image. Subsequently, Noise2Void [25] uses a masking technique to denoise images, in which the neural network was employed to learn how to fill in pixel gaps within the noisy image. Because this method only denoises the underlying picture, it's unable to learn the noise distribution. Although Noise2Void model was trained on large image dataset with the same noise level, it may be adapted to denoise single similar image without extra inputs and weights updating. Noise2Self [26] further enhanced and generalized this fundamental approach. Besides, the Self2Self [27] as an unsupervised technique was developed for single picture denoising, which can achieve competitive performance to the fully trained approaches (i.e., Noisy2Clean). Recorrup2Recorrup (R2R) [28] outperformed Self2Self on real-world noise by corrupting the input picture into fresh noisy realization pairs. Noise2Sim [22] believes that an image usually has multiple self-similarities/repeated places (self-similarities/repeated). Given a patch within an image, one can always globally search one similar patch to construct similar image patch pairs for noise removal.

Noise2Noise first demonstrated that neural network models can be trained using only noisy images. Here, we brief introduce the main idea. The Noise2Noise requires the data to meet these two conditions: (a) each scene  $\mathbf{s}$  have at least two noisy images  $\mathbf{x}_1$  and  $\mathbf{x}_2$ ; (b) the noise within  $\mathbf{x}_1$  and  $\mathbf{x}_2$  must be independent and zero-mean. The training aim of

---

Noise2Noise optimization is to minimize the following loss

$$\operatorname{argmin}_{\theta} E_{\mathbf{s}, \mathbf{x}_1, \mathbf{x}_2} \|f_{\theta}(\mathbf{x}_1) - \mathbf{x}_2\|_F^2, \quad (1)$$

where  $f_{\theta}$  represents the training network and  $\theta$  is the network parameters. From above given conditions, different noise level image-pair is necessary for Noise2Noise training. However, such a strict condition is difficult to be satisfied, especially for spectral CT imaging.

## (2) Deep Learning in Spectral CT Reconstruction

To the best of our knowledge, deep learning based spectral CT reconstruction is difficult since there is no way to obtain sufficient high-quality images as references to train supervised networks. To obtain high-quality images, we previously proposed a U-net,  $L_p$ -norm, Total variation, Residual learning, and Anisotropic adaption (ULTRA) network [2], which uses the weighted anisotropic total variation as the regularization term for network training. The ULTRA has achieved good results in numerical simulations and clinical trials. However, the training of ULTRA requires labeled images, which makes it difficult to be adopted in practice.

Furthermore, as one of unsupervised deep learning techniques, the Noise2Sim attempts to denoise spectral CT images and already shows its great potential for addressing this task. The Noise2Sim borrowed the idea of Noise2Noise to construct pseudo-label by searching similar image-pairs. In this work, the spectral CT images of adjacent slices are treated as similar images. Assume two noisy images  $\mathbf{x}_1 = \mathbf{s} + \mathbf{n}_1$  and  $\mathbf{x}_2 = \mathbf{s} + \mathbf{n}_2 + \delta$ , where  $\delta$  is the difference between clean images,  $\mathbf{n}_1$  and  $\mathbf{n}_2$  are two independent and zero-mean noise images. The parameters  $\theta$  of the denoising network are optimized as:

$$\operatorname{argmin}_{\theta} E_{\mathbf{s}} \|f_{\theta}(\mathbf{s} + \mathbf{n}_1) - (\mathbf{s} + \mathbf{n}_2 + \delta)\|_2^2. \quad (2)$$

The noise assumption of Noise2Sim can be described as  $E[\mathbf{n}_2 | \mathbf{n}_1 + \mathbf{s}] = E[\mathbf{n}_2 | \mathbf{s}] = \mathbf{0}$ . Through searching the similar image patches,  $E[\delta | \mathbf{n}_1 + \mathbf{s}] \approx \mathbf{0}$  can be ensured in practice. That is, Noise2Sim is approximately equivalent to Noise2Noise when the images are similar enough.

## B. Spectral2Spectral Framework

### (1) Overall Architecture

Figure 1(a) shows the proposed Spectral2Spectral framework, which is similar to the traditional iterative optimization reconstruction method. Regarding the network architecture, it can be divided into three modules: algebraic iteration (i.e., simultaneous iteration reconstruction technique, SIRT), novel unsupervised network design, and loss function optimization. Specifically, the classical SIRT reconstruction technique is first performed on the input sinogram to backward initial reconstruction images. Second, an unsupervised network is employed to approximate the intermediate reconstruction results.

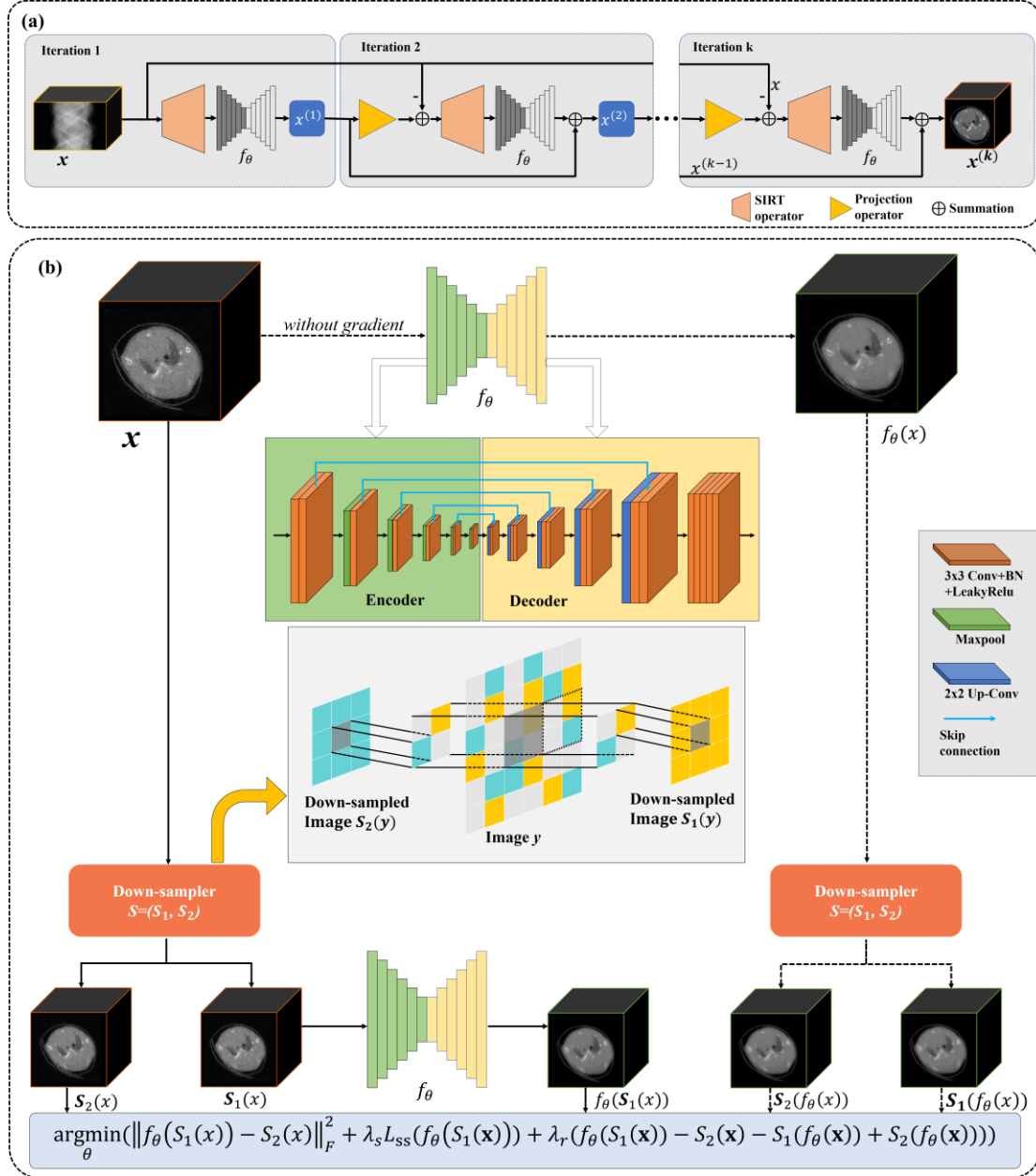


Fig. 1. The flowchart of Spectral2Spectral. (a)The workflow of the proposed method, (b) the training process of our proposed network.

Here, our unsupervised network is adaptively updated with iteration, which means our Spectral2Spectral network can effectively captures image features and information. To characterize the similarity and correlations across energy spectral domains, a novel loss function is proposed to enhance image feature recovery and detail fidelity. In fact, we can further clearly clarify our Spectral2Spectral with three basic theories: reconstruction optimized theory, unsupervised denoising theory, and regularization optimization theory.

## (2) Optimized Reconstruction

The image reconstruction of a typical spectral CT system with cone-beam geometry can

be formulated as:

$$\mathbf{y}_i = \mathbf{A}\mathbf{x}_i + \boldsymbol{\epsilon}_i, \quad i = 1, \dots, I, \quad (3)$$

where  $\mathbf{y}_i \in R^N$  represents the projection data from  $i^{th}$  ( $1 \leq i \leq I$ ) energy bin, and  $I$  represents the number of energy channels.  $N$  is the product of the PCD elements and the number of sampling angles.  $\boldsymbol{\epsilon}_i \in R^N$  represents noise within measurements,  $\mathbf{x}_i \in R^J$  ( $J = H_1 \times H_2 \times H_3$  where  $H_1$ ,  $H_2$  and  $H_3$  represent the size of reconstructed volumetric image), and  $\mathbf{A} \in R^{N \times J}$  is the CT system matrix. Theoretically speaking, the solution can be achieved by operating the matrix inverse over Eq. (3). However, it is not applicable in practice since the system matrix is too huge to be implemented directly. Rather than to solve this problem directly, it can be iterative handled by minimizing an optimization function

$$\min_{\{\mathbf{x}_i\}_{i=1}^I} \frac{1}{2} \sum_{i=1}^I \|\mathbf{y}_i - \mathbf{A}\mathbf{x}_i\|_F^2, \quad (4)$$

where  $\|\cdot\|_F^2$  represents Frobenius norm. To stabilize reconstruction results for ill-posed problems, the regularization term that characterizes prior knowledge can be incorporated into Eq. (4), and we have

$$\mathcal{X}^* = \underset{\mathcal{X}}{\operatorname{argmin}} \left( \frac{1}{2} \sum_{i=1}^I \|\mathbf{y}_i - \mathbf{A}\mathbf{x}_i\|_F^2 + \lambda \Phi(\mathcal{X}) \right), \quad (5)$$

where  $\frac{1}{2} \sum_{i=1}^I \|\mathbf{y}_i - \mathbf{A}\mathbf{x}_i\|_F^2$  represents data consistency term,  $\Phi$  represents the regularization term,  $\lambda$  is a factor to balance the data fidelity and regularization term, and  $\mathcal{X}$  represents one tensor formulating by rolled all energy-channel images  $\{\mathbf{x}_i\}_{i=1}^I$ . The compressed sensing theory does not explicitly point out the specified sparse transformation, and it only requires that the observation matrix should meet the RIP (Restricted Isometry Property) conditions. That means there are many different possible sparse models based on the compressed sensing theory. The regularization term is generally the most essential part of optimization model. Different regularization priors can induce different image reconstruction algorithms. The most popular regularization priors include the total variation (TV) and its variants, the tight framelet, dictionary based sparse representation, nonlocal means, and low-rank matrix factorization [29-32]. The goal of Eq. (5) is to determine an optimal solution by minimizing the entire objective function. The split-Bregman method can be employed to solve this problem. Here, we first introduce a parameter  $\mathcal{Z}$  to re-express Eq. (5) as follows

$$\{\mathcal{X}^*, \mathcal{Z}^*\} = \underset{\{\mathcal{X}, \mathcal{Z}\}}{\operatorname{argmin}} \left( \frac{1}{2} \sum_{i=1}^I \|\mathbf{y}_i - \mathbf{A}\mathbf{x}_i\|_F^2 + \lambda \Phi(\mathcal{Z}) \right), \quad \text{subject to } \mathcal{Z} = \mathcal{X}. \quad (6)$$

This constrained optimization problem can be converted into an unconstrained optimization problem:

$$\{\mathcal{X}^*, \mathcal{Z}^*\} = \underset{\{\mathcal{X}, \mathcal{Z}\}}{\operatorname{argmin}} \left( \frac{1}{2} \sum_{i=1}^I \|\mathbf{y}_i - \mathbf{A}\mathbf{x}_i\|_F^2 + \lambda \Phi(\mathcal{Z}) + \frac{\lambda_1}{2} \|\mathcal{Z} - \mathcal{X}\|_F^2 \right). \quad (7)$$

Eq. (7) can be divided into two sub-problems:

$$\mathcal{X}^{(k+1)} = \underset{\mathcal{X}}{\operatorname{argmin}} \left( \frac{1}{2} \sum_{i=1}^I \|\mathbf{y}_i - \mathbf{A}\mathbf{x}_i\|_F^2 + \frac{\lambda_1}{2} \|\mathcal{X} - \mathcal{Z}^{(k)}\|_F^2 \right), \quad (8)$$

$$\mathbf{z}^{(k+1)} = \underset{\mathbf{z}}{\operatorname{argmin}} \left( \frac{\lambda_1}{2} \|\mathbf{z} - \mathbf{x}^{(k+1)}\|_F^2 + \lambda \Phi(\mathbf{z}) \right), \quad (9)$$

where  $k$  indicates the iteration number. Eq. (8) can be solved by operating the partial derivative of  $\mathbf{x}$ , that is

$$\mathbf{A}^T \sum_{i=1}^I (\mathbf{A}\mathbf{x}_i - \mathbf{y}_i) + \lambda_1 (\mathbf{x} - \mathbf{z}^{(k)}) = 0. \quad (10)$$

where  $\mathbf{A}^T$  represents the transpose of system matrix. Eq. (10) can be reformatted to:

$$(\mathbf{A}^T \mathbf{A} + \lambda_1) \mathbf{x} = (\mathbf{A}^T \mathbf{A} + \lambda_1) \mathbf{x}^{(k)} + \mathbf{A}^T (\mathbf{y} - \mathbf{A} \mathbf{x}^{(k)}) + \lambda_1 (\mathbf{z}^{(k)} - \mathbf{x}^{(k)}), \quad (11)$$

then  $\mathbf{x}$  can be obtained by an iterative method:

$$\mathbf{x}^{(k+1)} = \mathbf{x}^{(k)} + (\mathbf{A}^T \mathbf{A} + \lambda_1)^{-1} \{ \mathbf{A}^T (\mathbf{y} - \mathbf{A} \mathbf{x}^{(k)}) + \lambda_1 (\mathbf{z}^{(k)} - \mathbf{x}^{(k)}) \}. \quad (12)$$

In fact, Eq. (12) is the conventional iterative reconstruction formula with appropriate approximation to  $(\mathbf{A}^T \mathbf{A} + \lambda_1)^{-1}$ , which can be updated with SIRT reconstruction technique. Eq. (9) is a typical image restoration problem, and here one unsupervised convolutional neural network is proposed to adaptively approximate its solution. Based on the above theoretical analysis, adding deep learning to iterative reconstruction has a solid theoretical basis.

### (3) Unsupervised Approximation Network

For the image restoration problem Eq. (9), the neural network is an effective strategy for optimization. In fact, the intermediate raw image is usually tarnished by noises and artifacts in spectral CT. It can be generated from the joint distribution  $p(\mathbf{x}_i, \mathbf{n}) = p(\mathbf{x}_i)p(\mathbf{n}|\mathbf{x}_i)$ . The aim of neural network  $f_{\theta}$  is to learn a mapping function recovering the clean image from noisy image, where  $f$  is parameterized by the weights  $\theta$ .

The iterative reconstruction framework is usually fixed, and the final reconstruction of spectral CT often depends on the design of unsupervised denoising network. Our approximation network is inspired by a recently published approach called Neighbor2Neighbor [33] where the neural network learns to map adjacent pixels in the image to one-another, and the adjacent pixels tend to have a similar underlying signal. Here, we assume there are only small differences within a clean image pair:  $\mathbf{s}$  and  $\mathbf{s} + \delta$ , and  $\delta \rightarrow 0$ .  $\mathbf{x}_1$  and  $\mathbf{x}_2$  are the noisy versions of  $\mathbf{s}$  and  $\mathbf{s} + \delta$ , respectively. The following equation is established

$$E_{s, \mathbf{x}_1} \|f_{\theta}(\mathbf{x}_1) - \mathbf{s}\|_F^2 = E_{s, \mathbf{x}_1, \mathbf{x}_2} \|f_{\theta}(\mathbf{x}_1) - \mathbf{x}_2\|_F^2 - \sigma_{x_2}^2 + 2\delta E_{s, \mathbf{x}_1} (f_{\theta}(\mathbf{x}_1) - \mathbf{s}). \quad (13)$$

Please refer to [33] for proof of Eq.(13). From Eq. (13), it can be found that when  $\delta \rightarrow 0$ ,  $2\delta E_{s, \mathbf{x}_1} (f_{\theta}(\mathbf{x}_1) - \mathbf{s}) \rightarrow 0$ . This means  $(\mathbf{x}_1, \mathbf{x}_2)$  training pair can be used as an approximation of Noise2Noise. Therefore, if one finds the proper image pair  $\mathbf{x}_1$  and  $\mathbf{x}_2$  satisfying the property of "similar but not identical" ( $\delta \rightarrow 0$ ), the denoising network can be trained. The essential problem is to construct such "*similar but not identical*" image pairs. One possible way of searching "*similar but not identical*" image pair for a single noisy image is down-sampling. The feasible sub-images can be sampled from adjacent but different positions of original noisy image. Such sub-images will satisfy the condition "*similar but not identical*" and ensure their difference is small and their corresponding clean images are not the same. Specifically, to sample a noisy image  $\mathbf{x}$ , a pair of nearest adjacent down-sampler  $(S_1(\cdot), S_2(\cdot))$

)) are used to generate  $(S_1(\mathbf{x}), S_2(\mathbf{x}))$ . To train a neural network in a Noise2Noise fashion, Eq. (1) can be rewritten as

$$\operatorname{argmin}_{\theta} E_{s, \mathbf{x}} \|f_{\theta}(S_1(\mathbf{x})) - S_2(\mathbf{x})\|_F^2. \quad (14)$$

Because the sampling positions of  $S_1(\mathbf{x})$  and  $S_2(\mathbf{x})$  are different, that is

$$E_{\mathbf{x}|\mathbf{s}}(S_1(\mathbf{x})) \neq E_{\mathbf{x}|\mathbf{s}}(S_2(\mathbf{x})). \quad (15)$$

If we only employ Eq. (14) to train the network directly, it is unlikely to yield optimal results but over-smoothed images. This situation can be corrected by adding a regularization term  $L_r$  to the loss function. For an ideal denoise network, it should satisfy the following two conditions:

$$\begin{cases} f_{\theta}(\mathbf{x}) = \mathbf{s} \\ f_{\theta}(S_i(\mathbf{x})) = S_i(\mathbf{s}), i \in \{1, 2\} \end{cases}. \quad (15)$$

Thus, we obtain the following expression

$$\begin{aligned} L_r &= E_{\mathbf{x}|\mathbf{s}} \left\{ f_{\theta}(S_1(\mathbf{x})) - S_2(\mathbf{x}) - (S_1(f_{\theta}(\mathbf{x})) - S_2(f_{\theta}(\mathbf{x}))) \right\} \\ &= S_1(\mathbf{s}) - E_{\mathbf{x}|\mathbf{s}}\{S_2(\mathbf{x})\} - (S_1(\mathbf{s}) - S_2(\mathbf{s})) = S_2(\mathbf{s}) - E_{\mathbf{x}|\mathbf{s}}\{S_2(\mathbf{x})\}, \end{aligned} \quad (17)$$

and  $L_r$  can be considered as a regularization term for Eq. (14)

$$\operatorname{argmin}_{\theta} (E_{s, \mathbf{x}} \|f_{\theta}(S_1(\mathbf{x})) - S_2(\mathbf{x})\|_F^2 + \lambda_r L_r). \quad (18)$$

$L_r$  is used to prevent the denoising network from overfitting, and  $\lambda_r > 0$  should gradually increase with the training progresses. Eq. (18) can be considered as fundamental loss function of denoising network.

#### (4) Spectral Regularization Prior

The loss function in Eq. (18) usually causes image being over-smoothed as well as finer structures losing, a new regularization term is introduced to recover blurry details. To further explore the sparse potential of spectral CT reconstruction, it is an effective way to incorporate image-spectral characteristic into the loss function. First, it is well known that different energy channel images have different grey intensities, but they share the same image structures since channel-wise images are from the same physical object. It seems feasible to establish a unique loss to explore the relationship across image-spectral space. Empirically, the image from full-spectrum by adding the photons of all energy bins often provides a higher SNR than that obtained from a single energy channel. Therefore, the full-spectrum reconstructed image can be treated as the reference to calculate SSIM [34]. By considering the relationship within spectral-cross domain, we propose a structural similarity (SSIM) loss function  $L_{SS}$  to characterize the similarity within image-spectral domain. Here, the SSIM can be given as

$$SSIM(\mathbf{x}, \mathbf{y}) = \frac{(2\mu_{\mathbf{x}}\mu_{\mathbf{y}} + C_1)(2\sigma_{\mathbf{xy}} + C_2)}{(\mu_{\mathbf{x}}^2 + \mu_{\mathbf{y}}^2 + C_1)(\sigma_{\mathbf{x}}^2 + \sigma_{\mathbf{y}}^2 + C_2)}, \quad (19)$$

where  $\mathbf{x}$  and  $\mathbf{y}$  are two images,  $\mu_{\mathbf{x}}$  and  $\sigma_{\mathbf{x}}^2$  respectively represent the mean and the variance of  $\mathbf{x}$ , and  $\sigma_{\mathbf{xy}}$  is the covariance of  $\mathbf{x}$  and  $\mathbf{y}$ . However, Eq. (19) cannot be used to spectral CT directly since different energy bins have different intensities. Indeed, different energy-bin images always have different mean values. However, if the channel-wise spectral images can



be normalized using their corresponding mean value, we can further normalize images to calculate SSIM. To address this issue, let  $\mathbf{x}^o$  be the network intermediate output,  $\mathbf{x}_i^o$  is  $i$ -th energy bin image of  $\mathbf{x}^o$ , and  $\mathbf{x}_{i\text{-norm}}^o$  represents the normalization of  $\mathbf{x}_i^o$ . Let  $\mathbf{x}_{\text{ref}}$  be normalized image from full-spectrum average image. Then we can express the  $L_{SS}$  as

$$L_{SS} = 1 - \frac{1}{I} \sum_{i=1}^I SSIM(\mathbf{x}_{i\text{-norm}}^o, \mathbf{x}_{\text{ref}}). \quad (20)$$

Regarding the normalization, the following formula is used in this study

$$\mathbf{x}_{i\text{-norm}}^o = \frac{\mathbf{x}_i - \min(\mathbf{x}_i)}{\max(\mathbf{x}_i) - \min(\mathbf{x}_i)}, \quad (21)$$

where  $\max(\cdot)$  represents the maximum value and  $\min(\cdot)$  represents the minimum value. Finally, the loss function can be given as

$$\operatorname{argmin}_{\theta} (E_{S, \mathbf{x}} \|f_{\theta}(S_1(\mathbf{x})) - S_2(\mathbf{x})\|_F^2 + \lambda_s L_{SS} + \lambda_r L_r). \quad (22)$$

Eq. (22) shows that two regular terms  $L_{SS}$  and  $L_r$  play different roles in the process of network training.  $L_r$  is good at image features recovery to avoid over smooth, and  $L_{SS}$  benefits to speedup the network fitting process and prevent detail losing.

The overall flow of our network is shown in the Figure 1(b). For a given input image, we first down-sample the original images by employing a neighbor sub-sampler pair  $S = (S_1, S_2)$  to generate a similar image pair  $(S_1(\mathbf{x}), S_2(\mathbf{x}))$ . Then, using  $\mathbf{x}$  and  $S_1(\mathbf{x})$  as the neural network inputs, we can further obtain the output  $f_{\theta}(\mathbf{x})$  and  $f_{\theta}(S_1(\mathbf{x}))$ . Down-sampling  $f_{\theta}(\mathbf{x})$  to generate  $S_1(f_{\theta}(\mathbf{x}))$  and  $S_2(f_{\theta}(\mathbf{x}))$ , one can calculate the loss function using Eq. (22). As for the neural network, we employ the U-net to make full use of the characteristics of the image, and the architecture is shown in Figure 1(b). To construct the aforementioned down-sampler, Figure 1(b) provides an intuitive diagram. For a given image  $\mathbf{y}$ , it is divided into several  $2 \times 2$  image patches firstly. For each image patch, two neighboring pixels are randomly chosen. For example, the pixel marked in yellow is taken as a pixel of a down-sampled image  $S_1(\mathbf{y})$ , and the other pixel marked in cyan is taken as a pixel of another down-sampled image  $S_2(\mathbf{y})$ .

### III. Experiments and Results

In this section, we first introduce the spectral CT dataset for reconstruction, including data preparation and neural network configuration. To validate our proposed unsupervised neural network for reconstruction, the conventional iteration reconstruction by incorporating TV prior (i.e., TVM) is selected as one of the comparison methods. In addition, to further demonstrate our method over other unsupervised reconstruction methods, two post-processing methods are implemented (i.e., Noise2Sim [22] and Neighbor2Neighbor [33]) to make a fair evaluation. Since it is difficult to obtain clean labels, we only apply unsupervised deep learning algorithms for high-quality reconstruction. Noise2Sim has shown its capability in spectral CT reconstruction, which is chosen as comparison. Another approach is Neighbor2Neighbor, which has shown to be successful in reducing natural image noise. Experimental results on the physical phantom and two preclinical mice demonstrate the advantages of our proposed method in spectral CT reconstruction.

---

## A. Spectral Dataset and Network Configuration

### (1) Preclinical Mice Data

To obtain spectral CT preclinical dataset, a spectral CT imaging system based on a photon counting detector is employed to scan mice in our first study as shown in Figure 2(a), and a mouse is shown in Figure 2(b). The photon-counting detector (the ME series of SANTIS 0804) manufactured by DECTRIS contains four fully independently adjustable energy gating thresholds. It consists of  $515 \times 257$  pixels with each of detector pixel covering an area of  $150 \times 150 \mu\text{m}^2$ . The SANTIS 0804 is a Hybrid Photon Counting (HPC) detector, and it can configure high-resolution mode and multi-energy mode. The multi-energy mode is set to collect the projections, where the maximum tube voltage is 160kVp, and the maximum input photon counting rate is  $4.0 \times 10^8$  photons/s/mm<sup>2</sup>.

The scanned mice have been injected with relevant reagents to keep it sleeping during the scanning process. Their weights and lengths are roughly 160-180g and 10 cm. The distance starting from x-ray source to the detector and object are 350mm and 210mm, respectively. The emitting x-ray spectrum with 70kVp is divided into five energy bins: [20, 30) KeV, [30, 40) KeV, [40, 50) KeV, [50, 60) KeV and [60, 70]KeV. There is 250 projection angles uniformly distributed over  $360^\circ$ . For fan-beam geometry of the central slice, the projection size is  $512 \times 250 \times 5$ , where 250 is the number of projection views.

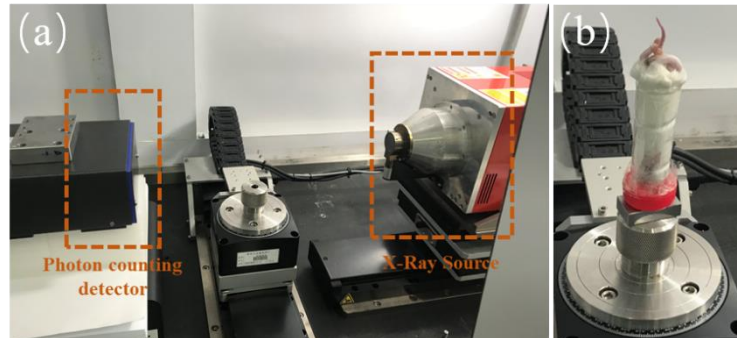


Fig. 2 The spectral CT imaging system and experiment materials. (a) is the spectral CT imaging system based on photon counting detector and (b) is the mice specimen.

### (2) Network Configuration

The programming language used in the experiments is Python 3.6, the U-Net network is implemented based on the deep learning framework Pytorch 1.7.0, and the implementation of SIRT is based on the Astra Toolbox 1.9.0dev. The post-processing method is to denoise the result of SIRT reconstruction, where the number of SIRT iterations is 50. The hardware platform configuration for running each network is as follows: Intel i5-9600kf CPU, Nvidia TITAN V (12GB / Nvidia) GPU, and 16G DDR4 RAM. For each network training, the number of epochs is set to 50, the learning rate is  $1.0 \times 10^{-4}$  and decreased to 90% per 10 epochs, and the Adam method is employed to optimize the network.

---

## B. Experimental Results

### (1) Preclinical Mice

To demonstrate the excellent reconstruction performance of Spectral2Spectral, Figs. 5 and 6 show the reconstruction results with five energy bins of two different slices from two mice, respectively. Here, the extracted ROIs are also highlighted. The 1<sup>st</sup> -5<sup>th</sup> columns represent five different energy bins of 25-35keV, 35-45keV, 45-55keV, 55-65keV and 65-75keV, respectively.

It can be seen from Fig. 3 that the image reconstructed using TVM has the strongest noise. Moreover, the image details in 4<sup>th</sup> and 5<sup>th</sup> energy bins have been deteriorated, and bone features are difficult to be distinguished. The image qualities of the two post-processing methods based on unsupervised deep learning are significantly better than that obtained by TVM. These results are tarnished with less noises and further provide sharper edges and more image details. However, in the last two channels, they don't work well. Particularly, as indicated by the green arrow in the second row, the results of Noise2Sim work well in non-edge places without grayscale abrupt changes, but there is obvious noise at the junction of soft tissue and bone, and there is a situation where the boundary is blurred. The Noise2Sim adopts the spatial similarity between adjacent layers of the image to be reconstructed, and it does not use the similarity between different energy bins along the spectral dimension. Furthermore, Noise2Sim performs well when the noise levels of all energy channels are consistent. However, when the noise levels are drastically different, the denoising effect suffers. Regarding neighbor2neighbor, compared with Noise2Sim, it has less noises and clearer tissue structures. However, as indicated by the green arrows in the third row, the grayscale difference between bone and soft tissue is small, and it cannot be clearly identified. The reason for this phenomenon is that neighbor2neighbor does not need adjacent layers to construct training pairs, so there is no spatial similarity as the basis for network training, and the geometric similarity between energies is not used. The projection data's energy range is limited, resulting in a lot of noises and uneven distribution. Denoising the image alone is not enough to restore the bone structures. In contrast, our proposed Spectral2Spectral recovers image features more significantly than compressed sensing reconstruction and other deep reconstruction networks for spectral CT imaging. No matter in which energy channel, image edges and tissue structures are clearer.

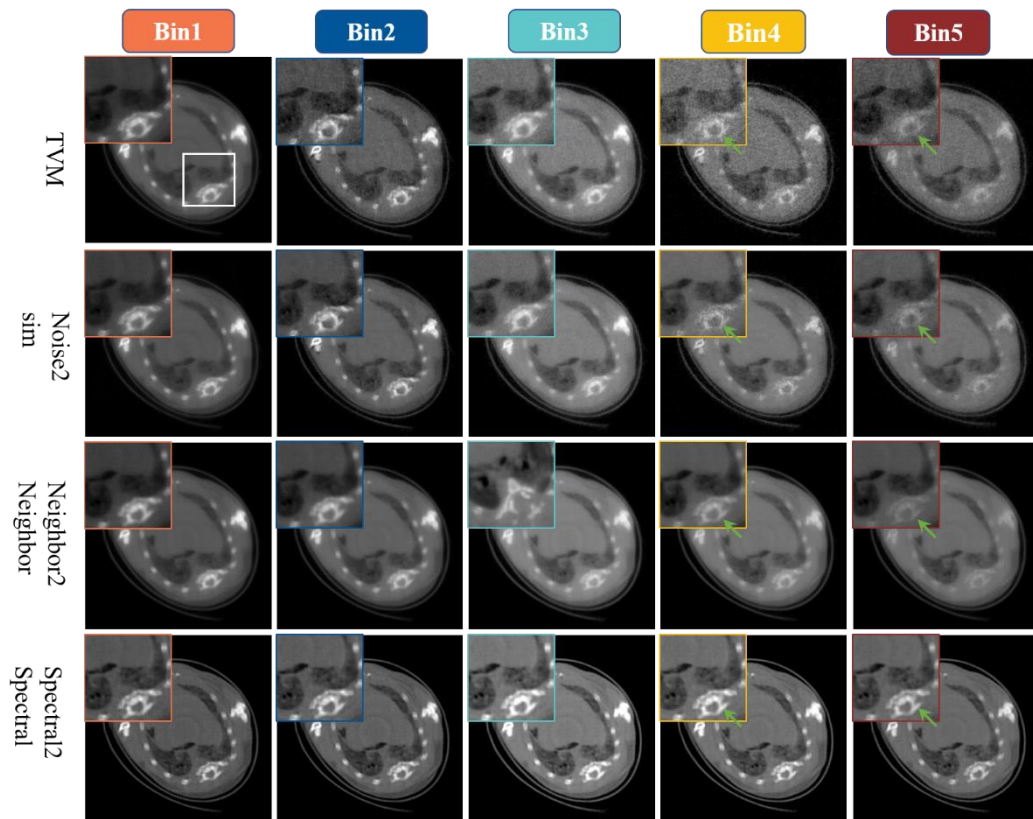


Fig. 3 Reconstruction results of case 1 from mice 1# using different reconstruction algorithm, ROI is located at the white box. From 1<sup>st</sup>-5<sup>th</sup> columns, the display windows are [0,0.007], [0,0.0045], [0,0.003], [0,0.003], and [0,0.003].

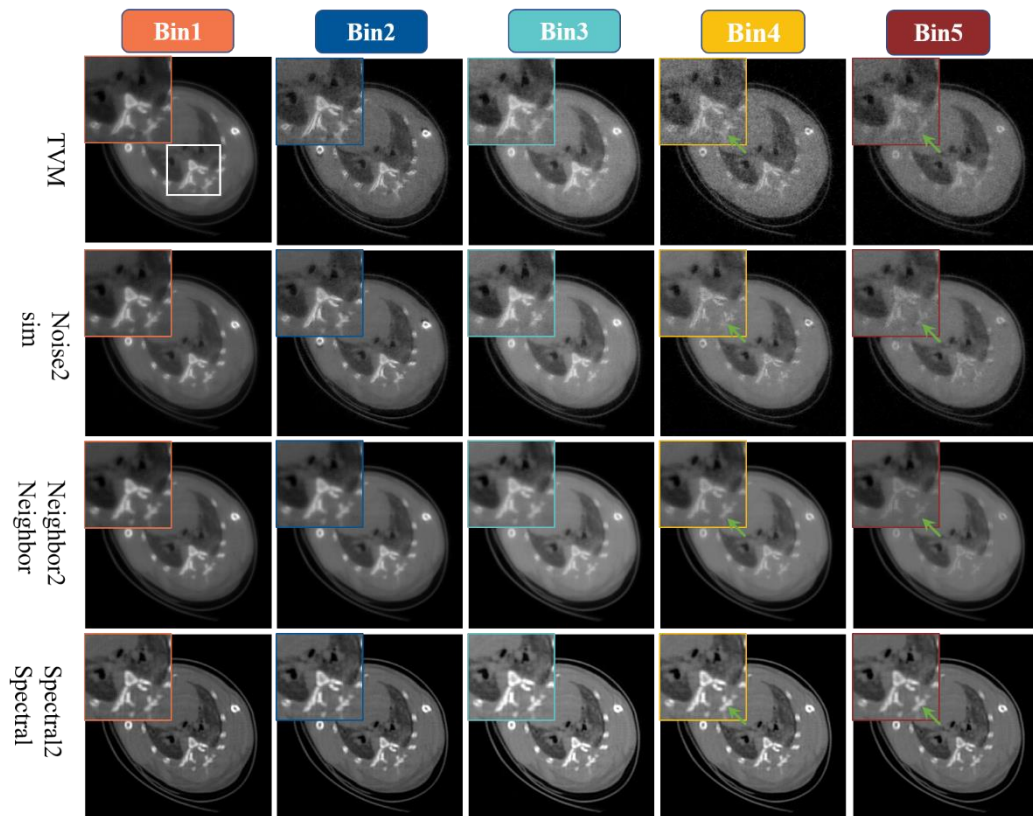


Fig. 4 Reconstruction results of case 1 from mice 2# using different reconstruction algorithm,

ROI is located at the white box. From 1<sup>st</sup>-5<sup>th</sup> columns, the display windows are [0,0.007], [0,0.0045], [0,0.003], [0,0.003], and [0,0.003].

Figures 5 and 6 also provide reconstruction results in terms of sagittal and coronal views. It can be seen from the red arrows in 5<sup>th</sup> energy-bin images in Figure 5, Spectral2Spectral provides the clearest bony structures. The coronal reconstructions shown in Figure 6 are also exciting. Spectral2Spectral can reconstruct some pronounced tissue structures, as indicated by the red box. For the reconstructed results in 3<sup>rd</sup>-5<sup>th</sup> energy-bins, TVM and Noise2Sim fail to clearly reconstruct the structures in the red boxes. Particularly, the bony structures in 5<sup>th</sup> energy-channel image are missing. Compared with Neighbor2Neighbor results, our Spectral2Spectral provides the clearest image edge and structures as well as the highest contrast.

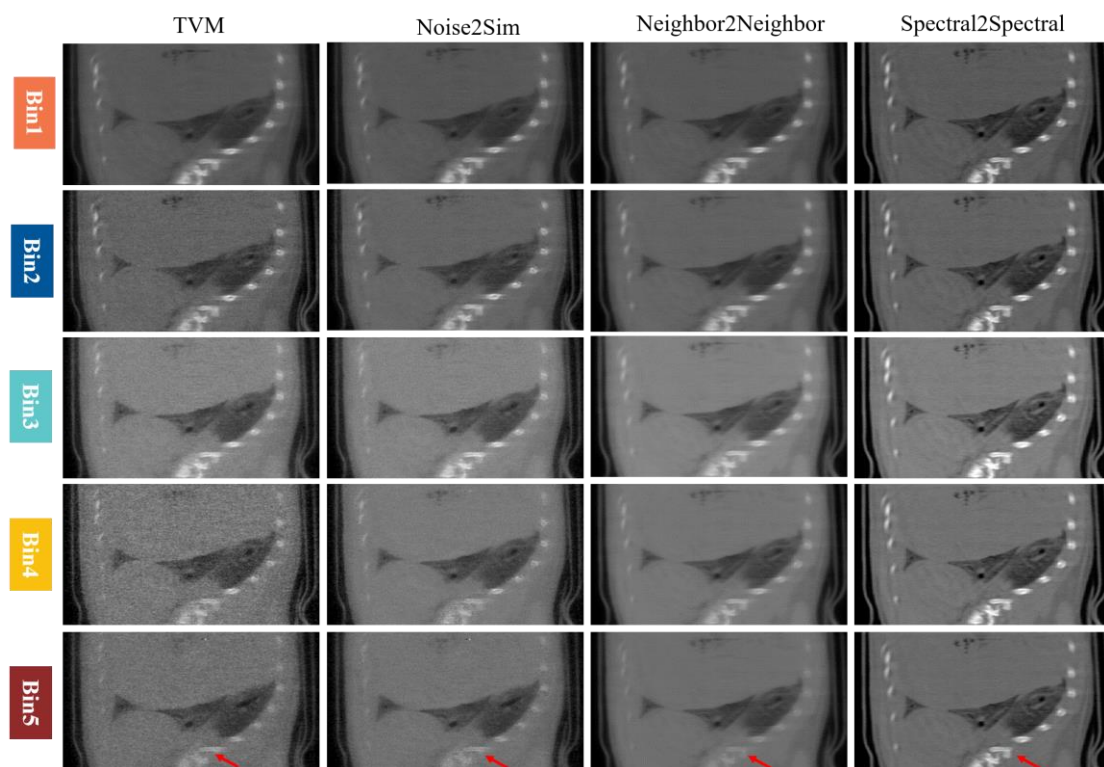


Fig. 5 The reconstruction results of one representative sagittal slice from mice 1#, and the display windows are set the same as Fig. 3.

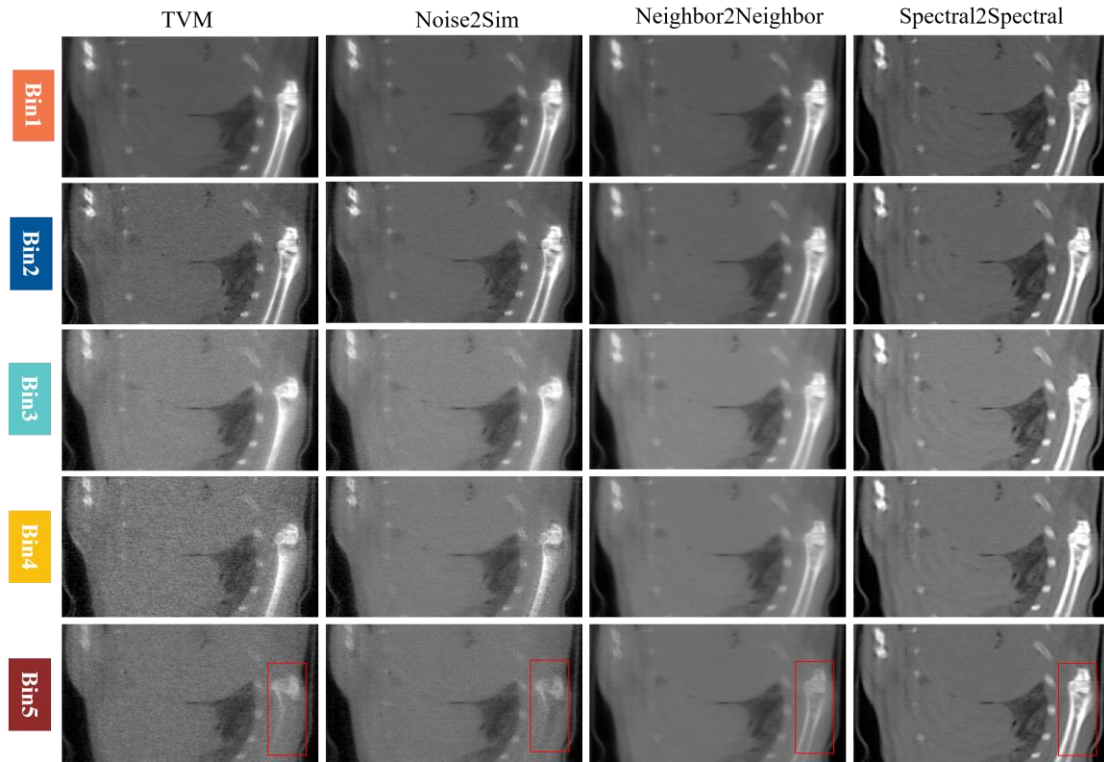


Fig. 6 The reconstruction results of one representative coronal slice from mice 1#, and the display windows are set as the same of Fig.3.

The aforementioned experimental results are limited to two-dimensional slices. Figure 9 provides a more intuitive impression in the 3D views, where ImageJ is used to display the reconstruction results of the 55-65 keV energy bin in the form of a thermograph. From Figure 7, we can see that our method provides the best image quality, which are reflected in the following two aspects. First, the overall noise level of the image is lower. For example, there are burrs between SIRT and Noise2Sim at the image edge. In addition, the bones of the first three methods contain fuzzy areas. On the contrary, the bone edges in our reconstruction results are clear. Second, our method can more clearly distinguish the differences between various tissues. The first three methods mix lung tissue and soft tissue together, which cannot be clearly identified. Spectral2Spectral has the most obvious lung organ tube structures.

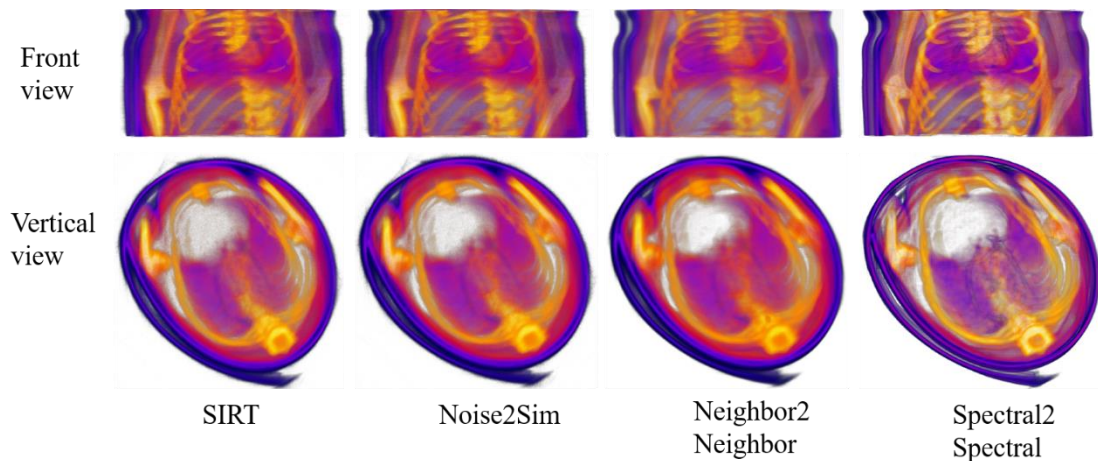


Fig. 7 The 3D visualization of different view from mice 1#

In addition to the visualization assessment, here we further introduce an image quality metrics to quantify the advantages of our proposed method. Different from low-dose CT reconstruction, there is no references to characterize reconstruction error. That means the PSNR, RMSE, and IFC [36] cannot be used for quantitative assessment. However, the above transverse slice has relatively simple geometric structures, and the sharpness of the image edge is used to measure the image quality may be feasible. Based on the work of [37], we define the sharpness measure of the image spatial resolution without reference. It is the percentage of the edges at which blur can be detected. The smaller its value is, the sharper the image edge is, and the better the spatial resolution is. Thus, the sharpness from the extracted ROI in Fig. 6 is selected as the basis to evaluate image quality. The results are shown in Table 1.

Table 1. Quantitative image evaluation results

Bins	TVM	Noise2Sim	Neighbor2Neighbor	Spectral2Spectral
1 <sup>st</sup>	0.2063	0.3126	0.0793	<b>0.0504</b>
2 <sup>nd</sup>	0.6562	0.4942	<b>0.0201</b>	0.0716
3 <sup>rd</sup>	0.6542	0.6909	0.1643	<b>0.0422</b>
4 <sup>th</sup>	0.7531	0.7953	0.2864	<b>0.0899</b>
5 <sup>th</sup>	0.7745	0.8125	0.5645	<b>0.1020</b>

Table 1 demonstrates the evaluation results are consistent with the visualization assessment generally. It can be seen that Noise2Sim is unclear than TVM in most energy-channel images, which demonstrates the Noise2Sim fail to provide clear edge structures. Compared with TVM and Noise2Sim, Neighbor2Neighbor improves reconstruction performance. However, our Spectral2Spectral has the best image quality in all energy bins, which means the image quality has been improved.

### C. Ablation Study

To evaluate different modules in our proposed method, the ablation studies are performed. First, the results in Fig. 8 demonstrate the effectiveness of the spectral regularization prior. From Fig. 8, our method can provide clearer image edges and structures, and it demonstrates the spectral regularization prior enhances image edges. Then, to illustrate the role of the optimization framework, the approximation neural network in the iteration framework is only considered as an image-domain post-processing neural network. In other words, there is no iteration in overall framework. The results in Fig.9 fully demonstrates that the iteration framework can provide more clear image details, and those are blurred in image-domain post-processing neural network.

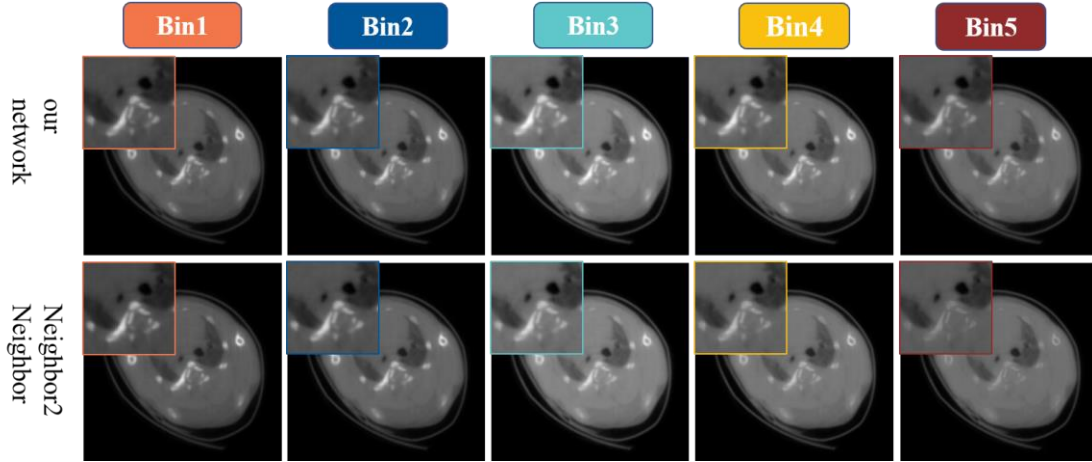


Fig. 8 Ablation study in terms of spectral regularization prior. 1<sup>st</sup>-2<sup>nd</sup> rows results are reconstructed with and without the spectral regularization prior.

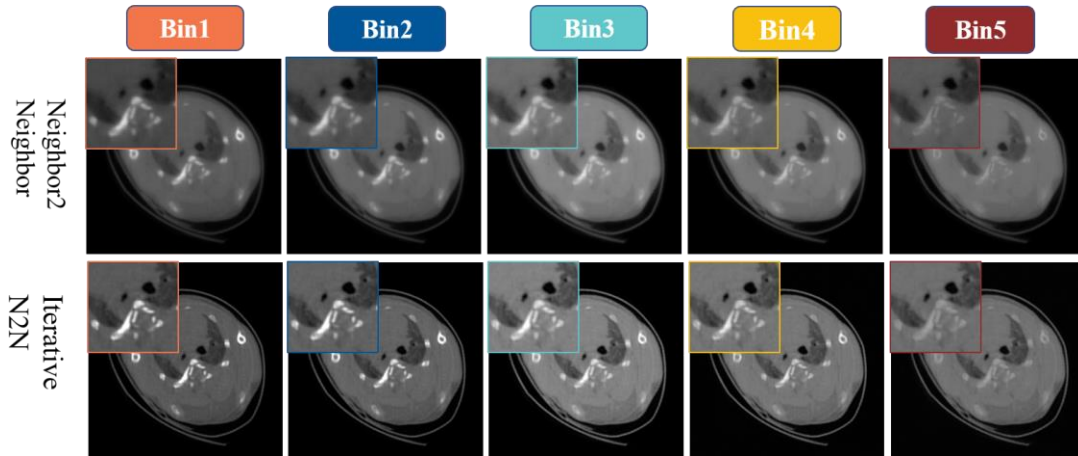


Fig. 9 Ablation study in terms of image-domain post-processing and iteration optimization. 1<sup>st</sup>-2<sup>nd</sup> rows represent reconstruction results from both the image-domain post-processing and iteration optimization.

## IV. Discussion and Conclusion

According to our experimental results, our proposed deep iterative reconstruction algorithm, *i.e.*, Spectral2Spectral, can obtain high-quality images from spectral CT data. More specifically, Spectral2Spectral has several key features and benefits. First, we unify the iterative reconstruction algorithm and deep learning into a framework, where the weights within network are adaptively updated with iteration without manually parameters adjustment. Second, we innovatively apply unsupervised deep learning to the field of spectral CT reconstruction. It can efficiently recover clear details from noisy images. Finally, to prevent the images from being too smooth, we exploit the structural similarity among the spectral CT images to fully train approximation network. Spectral2Spectral significantly improves reconstruction performance. Compared with compressed sensing-based reconstruction technique, Spectral2Spectral results provide high-quality images with less noise. Our method



---

outperforms the state-of-the-art neural network post-processing and compressed sensing methods.

The network structure in our study is U-Net, which is not the latest network structure. CNN-like networks have strong local feature extraction capabilities, but these networks cannot capture global feature information. In the follow-up research, we can try to combine self-attention-based architectures like Transformers[38] with CNN as a more powerful feature extractor. Second, we use the structural similarity among different energy channels to constrain the network training, without using some other prior information, such as the CT image sparsity and spatial similarity. Hence, more constraints can be added to further improve image quality. Third, we use the similarity between adjacent pixels to construct training pairs. In the further research, we should explore a new method to generate pseudo labels from the image itself according to the characteristics of spectral CT, so that the network can learn noise distribution more effectively.

In conclusion, we reconstruct spectral CT by combining deep learning with iterative reconstruction methods, and the reconstruction performance on narrow energy channels has been verified. It further demonstrates that deep learning can coexist with traditional reconstruction methods to obtain better image quality. It is believed that our proposed method has great potential in spectral CT reconstruction.

## Reference:

- 1 Donoho, D.L.: ‘Compressed sensing’, *IEEE Transactions on information theory*, 2006, 52, (4), pp. 1289-1306
- 2 Wu, W., Hu, D., Niu, C., Broeke, L.V., Butler, A.P., Cao, P., Atlas, J., Chernoglazov, A., Vardhanabhuti, V., and Wang, G.: ‘Deep learning based spectral CT imaging’, *Neural Networks*, 2021, 144, pp. 342-358
- 3 Zhang, Y., Mou, X., Wang, G., and Yu, H.: ‘Tensor-based dictionary learning for spectral CT reconstruction’, *IEEE transactions on medical imaging*, 2016, 36, (1), pp. 142-154
- 4 Wu, W., Zhang, Y., Wang, Q., Liu, F., Chen, P., and Yu, H.: ‘Low-dose spectral CT reconstruction using image gradient  $\ell_0$ -norm and tensor dictionary’, *Applied Mathematical Modelling*, 2018, 63, pp. 538-557
- 5 Cueva, E., Meaney, A., Siltanen, S., and Ehrhardt, M.J.: ‘Synergistic multi-spectral CT reconstruction with directional total variation’, *Philosophical Transactions of the Royal Society A*, 2021, 379, (2204), pp. 20200198
- 6 Kong, H., Lei, X., Lei, L., Zhang, Y., and Yu, H.: ‘Spectral CT reconstruction based on PICCS and dictionary learning’, *IEEE Access*, 2020, 8, pp. 133367-133376
- 7 Wang, Q., Wu, W., Deng, S., Zhu, Y., and Yu, H.: ‘Locally linear transform based three-dimensional gradient-norm minimization for spectral CT reconstruction’, *Medical Physics*, 2020, 47, (10), pp. 4810-4826
- 8 Zhou, Z., Zhang, X., Xin, R., Mao, L., Jia, J., Wei, S., Sheng, T., and Zheng, J.: ‘Direct iterative basis image reconstruction based on MAP-EM algorithm for spectral CT’, *Journal of Nondestructive Evaluation*, 2021, 40, (1), pp. 1-10
- 9 Chen, B., Zhang, Z., Xia, D., Sidky, E.Y., and Pan, X.: ‘Non-convex primal-

---

dual algorithm for image reconstruction in spectral CT', *Computerized Medical Imaging and Graphics*, 2021, 87, pp. 101821

10 Wang, G., Ye, J.C., and De Man, B.: 'Deep learning for tomographic image reconstruction', *Nature Machine Intelligence*, 2020, 2, (12), pp. 737-748

11 Chen, H., Zhang, Y., Zhang, W., Liao, P., Li, K., Zhou, J., and Wang, G.: 'Low-dose CT denoising with convolutional neural network', in Editor (Ed.)^(Eds.): 'Book Low-dose CT denoising with convolutional neural network' (IEEE, 2017, edn.), pp. 143-146

12 Chen, H., Zhang, Y., Kalra, M.K., Lin, F., Chen, Y., Liao, P., Zhou, J., and Wang, G.: 'Low-dose CT with a residual encoder-decoder convolutional neural network', *IEEE transactions on medical imaging*, 2017, 36, (12), pp. 2524-2535

13 Jin, K.H., McCann, M.T., Froustey, E., and Unser, M.: 'Deep convolutional neural network for inverse problems in imaging', *IEEE Transactions on Image Processing*, 2017, 26, (9), pp. 4509-4522

14 Ronneberger, O., Fischer, P., and Brox, T.: 'U-net: Convolutional networks for biomedical image segmentation', in Editor (Ed.)^(Eds.): 'Book U-net: Convolutional networks for biomedical image segmentation' (Springer, 2015, edn.), pp. 234-241

15 Zhang, Z., Liang, X., Dong, X., Xie, Y., and Cao, G.: 'A sparse-view CT reconstruction method based on combination of DenseNet and deconvolution', *IEEE transactions on medical imaging*, 2018, 37, (6), pp. 1407-1417

16 Kang, E., Min, J., and Ye, J.C.: 'A deep convolutional neural network using directional wavelets for low-dose X-ray CT reconstruction', *Medical physics*, 2017, 44, (10), pp. e360-e375

17 Han, Y., and Ye, J.C.: 'Framing U-Net via deep convolutional framelets: Application to sparse-view CT', *IEEE transactions on medical imaging*, 2018, 37, (6), pp. 1418-1429

18 Chun, Y., and Fessler, J.A.: 'Deep BCD-net using identical encoding-decoding CNN structures for iterative image recovery', in Editor (Ed.)^(Eds.): 'Book Deep BCD-net using identical encoding-decoding CNN structures for iterative image recovery' (IEEE, 2018, edn.), pp. 1-5

19 Chun, I.Y., Huang, Z., Lim, H., and Fessler, J.: 'Momentum-Net: Fast and convergent iterative neural network for inverse problems', *IEEE Transactions on Pattern Analysis and Machine Intelligence*, 2020

20 He, J., Wang, Y., and Ma, J.: 'Radon inversion via deep learning', *IEEE Transactions on Medical Imaging*, 2020, 39, (6), pp. 2076-2087

21 Zhu, B., Liu, J.Z., Cauley, S.F., Rosen, B.R., and Rosen, M.S.: 'Image reconstruction by domain-transform manifold learning', *Nature*, 2018, 555, (7697), pp. 487-492

22 Niu, C., Fan, F., Wu, W., Li, M., Lyu, Q., and Wang, G.: 'Suppression of Independent and Correlated Noise with Similarity-based Unsupervised Deep Learning', *arXiv preprint arXiv:2011.03384*, 2020

23 Trampert, J., and Leveque, J.J.: 'Simultaneous iterative reconstruction technique: physical interpretation based on the generalized least squares solution', *Journal of Geophysical Research: Solid Earth*, 1990, 95, (B8), pp. 12553-12559

---

24 Lehtinen, J., Munkberg, J., Hasselgren, J., Laine, S., Karras, T., Aittala, M., and Aila, T.: ‘Noise2Noise: Learning image restoration without clean data’, arXiv preprint arXiv:1803.04189, 2018

25 Krull, A., Buchholz, T.-O., and Jug, F.: ‘Noise2void-learning denoising from single noisy images’, in Editor (Ed.)<sup>(Eds.)</sup>: ‘Book Noise2void-learning denoising from single noisy images’ (2019, edn.), pp. 2129-2137

26 Batson, J., and Royer, L.: ‘Noise2self: Blind denoising by self-supervision’, in Editor (Ed.)<sup>(Eds.)</sup>: ‘Book Noise2self: Blind denoising by self-supervision’ (PMLR, 2019, edn.), pp. 524-533

27 Quan, Y., Chen, M., Pang, T., and Ji, H.: ‘Self2self with dropout: Learning self-supervised denoising from single image’, in Editor (Ed.)<sup>(Eds.)</sup>: ‘Book Self2self with dropout: Learning self-supervised denoising from single image’ (2020, edn.), pp. 1890-1898

28 Pang, T., Zheng, H., Quan, Y., and Ji, H.: ‘Recorrupted-to-Recorrupted: Unsupervised Deep Learning for Image Denoising’, in Editor (Ed.)<sup>(Eds.)</sup>: ‘Book Recorrupted-to-Recorrupted: Unsupervised Deep Learning for Image Denoising’ (2021, edn.), pp. 2043-2052

29 Sidky, E.Y., and Pan, X.: ‘Image reconstruction in circular cone-beam computed tomography by constrained, total-variation minimization’, *Physics in Medicine & Biology*, 2008, 53, (17), pp. 4777

30 Gao, H., Yu, H., Osher, S., and Wang, G.: ‘Multi-energy CT based on a prior rank, intensity and sparsity model (PRISM)’, *Inverse problems*, 2011, 27, (11), pp. 115012

31 Zhang, Y., Xi, Y., Yang, Q., Cong, W., Zhou, J., and Wang, G.: ‘Spectral CT reconstruction with image sparsity and spectral mean’, *IEEE transactions on computational imaging*, 2016, 2, (4), pp. 510-523

32 Sidky, E.Y., Kao, C.-M., and Pan, X.: ‘Accurate image reconstruction from few-views and limited-angle data in divergent-beam CT’, *Journal of X-ray Science and Technology*, 2006, 14, (2), pp. 119-139

33 Huang, T., Li, S., Jia, X., Lu, H., and Liu, J.: ‘Neighbor2neighbor: Self-supervised denoising from single noisy images’, in Editor (Ed.)<sup>(Eds.)</sup>: ‘Book Neighbor2neighbor: Self-supervised denoising from single noisy images’ (2021, edn.), pp. 14781-14790

34 Miaoshi, Wang, Yanbo, Zhang, Rui, Liu, Shuxu, Guo, Hengyong, and Yu: ‘An adaptive reconstruction algorithm for spectral CT regularized by a reference image’, *Physics in Medicine & Biology*, 2016

35 Wu, W., Chen, P., Vardhanabhuti, V.V., Wu, W., and Yu, H.: ‘Improved material decomposition with a two-step regularization for spectral CT’, *IEEE Access*, 2019, 7, pp. 158770-158781

36 Sheikh, H.R., Bovik, A.C., and De Veciana, G.: ‘An information fidelity criterion for image quality assessment using natural scene statistics’, *IEEE Transactions on image processing*, 2005, 14, (12), pp. 2117-2128

37 Narvekar, N.D., and Karam, L.J.: ‘A no-reference perceptual image sharpness

---

metric based on a cumulative probability of blur detection’, in Editor (Ed.)^(Eds.):  
‘Book A no-reference perceptual image sharpness metric based on a cumulative  
probability of blur detection’ (IEEE, 2009, edn.), pp. 87-91

38 Vaswani, A., Shazeer, N., Parmar, N., Uszkoreit, J., Jones, L., Gomez, A.N.,  
Kaiser, Ł., and Polosukhin, I.: ‘Attention is all you need’, Advances in neural  
information processing systems, 2017, 30